Scale and REV analyses for porosity and pore connectivity measures in undisturbed soil

J. Koestel*, M. Larsbo, N. Jarvis

Department of Soil and Environment, Swedish University of Agricultural Sciences, Box 7014, 750 07 Uppsala, Sweden

ARTICLE INFO

ABSTRACT

Soil samples with a volume of approximately 100 mL are commonly used for measuring soil properties needed to parameterize continuum models of transport processes in soils. The necessary assumption that the sampled soil volume corresponds to a representative elementary volume (REV) has only been occasionally tested. Furthermore, the few studies so far have focused on bulk properties such as porosity and bulk density and have not investigated the scale-dependence of pore-space connectivity, which is fundamental for transport properties such as the permeability of soil. In this study, we investigated the scale-dependence of morphologic properties of the soil pore-space in 25 undisturbed soil columns sampled from five different depths (8, 23, 33, 53 and 73 cm) from a field site in southern Norway (Skuterud). We conducted the analyses of scale-dependence on regions of interests of $40 \times 40 \times 40$ mm^3 from binarized X-ray images with a resolution of 40 μm. We focused our evaluation on imaged porosity and three measures of pore-space connectivity (the connection probability, the Euler-Poincaré number and the critical pore diameter). As pore network connectivity is scale-dependent and because the connectivity of large pores has a very strong impact on the soil permeability, we conducted our analyses considering three contrasting minimum pore diameters, namely 80, 250 and 500 μm.

We found that the pore connectivity improved with scale, predominantly due to the presence of pores with diameters of less than 0.25 mm. This stresses the importance of image resolution in scale analyses. We moreover observed that both the mean and the standard deviation of the critical pore diameter increased with scale, which may explain why the mean and standard deviation of the saturated hydraulic conductivity are often found to increase with scale. We detected an REV range for the macroporosity between approximately 15 and 65 mm. This range decreased with an increase in the minimum pore diameter considered. However, we also found evidence contradicting the existence of the detected REV range for the macroporosity due to a lack of statistical homogeneity. No REV range could be found for the three investigated connectivity measures, probably because the evaluated scales were too small. Based on our results we conclude that larger soil samples should be used to measure soil properties and investigate processes that depend on the pore network connectivity, such as permeability or water flow and long-range solute transport. We recommend that future studies should investigate REVs for connectivity measures and investigate which REV criteria are most meaningful in a continuum modelling context. Such studies are needed to evaluate whether REVs for transport properties are common in soils. If not, flow and transport models that explicitly account for heterogeneity are necessary.

1. Introduction

Simulation models are needed to estimate hydraulic state variables and flow processes in the vadose zone, which emerge from the underlying soil pore network architecture. State variables like water and air contents depend on the boundary conditions, porosity and the pore size distribution and on the pore connectivity. The largest pores tend to drain first when the matric potential decreases. The nature of the pore connection determines whether there is water entrapment during the

draining process (or air entrapment during wetting towards saturation). Flow, in turn, is influenced by all of the above. Larger porosities and pore diameters are associated with larger flow velocities, such that $q \propto \varphi_{eff} d_s^2$ (Berg, 2014) with q (mm h^{-1}) as the flow rate, φ_{eff} (mm^3 mm^{-3}) as the effective porosity and d_s (mm) as a characteristic length (pore diameter). Large pores that are disconnected from the rest of the soil pore space, if such pores occur, would obviously not allow any flow at all. At the other extreme, large water-filled pores that are continuous across the considered soil domain can dominate the flow

---

(Beven and Germann, 1982; Koestel et al., 2018).

The hydraulic properties of soils are determined by the geometry of pore networks. Measuring and modelling soil hydraulic state variables and flows at the pore scale is the subject of ongoing research (Koestel and Larsbo, 2014; Sammartino et al., 2015; Scheibe et al., 2015). Such approaches are necessary to advance our scientific understanding of soil water processes. However, with current technologies, explicit pore-scale model applications are unrealistic and impractical at larger scales, as they require too much computational power and are impossible to parameterize by direct measurements. Instead, an approach to upscale pore-scale processes is required (Pachepsky and Hill, 2017). Here, continuum simulation modeling (Köhne et al., 2009) is commonly employed and will most likely remain dominant in the foreseeable future. This approach helps solve an obvious dilemma. The hydraulic properties of bulk soil volumes, which emerge from pore-scale processes, are much easier to measure than the highly hierarchical and complex pore network structures. The continuum approach provides a theoretical framework that allows modelling flow and transport processes through porous media by employing the properties of local bulk volumes. Single, effective values thereby summarize a property emerging from the local pore-space architectures, e.g. the mean porosity represents the pore-volume fraction of a local bulk soil volume.

The continuum approach postulates the existence of representative elementary volumes (REV). Bachmat and Bear (1986) define an REV as a volume around a point in which "all averaged geometrical characteristics of the microstructure in a porous material at any point of the porous medium domain are single valued functions of the location of that point … but independent of the size of the volume". Moreover, the characteristics inside the REV must be statistically homogenous in order to be averaged. More practically, an REV can be found by starting at an arbitrary point within a considered domain of interest and expanding a volume centered on that point. The REV range, if it exists, includes scales for which the effective property of interest (e.g. porosity) is constant with the change of the considered volume. To qualify as an REV the volume needs to be i) large enough so that the effective property does not change when the volume is slightly increased and ii) small enough so that it does not include larger scale changes in the effective property, e.g. a drift in porosity due to macroscopic heterogeneities such as a transition between different horizons in a soil profile or between different soil types in a landscape. In the latter case, the requirement of statistical homogeneity would be violated. In the following, we refer to these scale boundaries that define an REV range as the lower, l_{min} (mm), and the upper boundary, l_{max} (mm). It is necessary to investigate both l_{min} and l_{max} to validate the existence of an REV range, because it cannot be ruled out that $l_{max} \leq l_{min}$ (Bachmat and Bear, 1986), in which case, no REV exists. A measurement from a bulk soil volume that fulfills the REV criteria is suitable for parameterizing continuum models (Baveye and Sposito, 1984).

The REV concept was developed during the 1950s and 1960s for an idealized porous medium (Hubbert, 1956; Raats and Klute, 1968a, 1968b). The existence of REVs in natural porous material such as soil has long remained hypothetical (Baveye and Sposito, 1984; Vogel, 2019). Early attempts to measure them were necessarily restricted to indirect or destructive approaches (Buchter et al., 1994; Lauren et al., 1988; VandenBygaart and Protz, 1999). With the advent of imaging techniques, such as X-ray tomography, it has become possible to investigate the existence of REVs non-invasively in three dimensions. One outcome of the early REV studies was that the criterion of zero fluctuation of the effective property upon inflation of the measurement volume was found to be unrealistic. This is both because measurements are not free from errors and in reality, natural porous media are heterogeneous, so there may be continuous gradual changes (drift) in properties due to spatial variations in, for example, texture or organic matter content. Therefore, Bachmat and Bear (1986) suggested allowing fluctuations in the effective property smaller than a pre-defined threshold value such that the REV assumption was approximately valid.

Zhang et al. (2000) referred to such volumes as statistical REVs. Most subsequently published studies on REVs followed this approach. We apply the same approach in this study denoting statistical REVs simply as 'REVs'.

It is striking that previous studies on REVs have focused on investigating the existence of a lower boundary (l_{min}) for possible REV ranges. Instead of evaluating the location of an upper boundary (l_{max}), they introduced criteria to test for statistical homogeneity at the lower REV boundary. Commonly, a measure of the maximum acceptable variance was calculated, e.g. the coefficient of variation between ROIs ("regions of interest") at scales larger than l_{min}. Approaches and criteria employed by these studies have varied slightly. As REV criteria, Zhang et al.(2000) proposed an approximately constant mean value with scale change and a CV of the investigated effective property of less than 0.2 for sub-volumes. Bruns et al. (2017) assumed a CV for sub-ROI properties of less than 0.1 as their criterion for the existence of an REV. Borges et al. (2018) instead used the maximum deviation between a measure in an ROI and the total investigated volume, which they required to be smaller than 10% for an REV. In contrast to these previous studies, Brown et al. (2000) used a single-factor analysis of variance at a significance level of 0.05 to test whether both the mean and the variance of an investigated property remained constant with an increasing size of the ROI. Costanza-Robinson et al. (2011), Li et al. (2009) and Wu et al., 2018 followed similar approaches as Brown et al. (2000).

Many of the early studies already investigated and reported REVs for more than one property of the porous medium, honoring theoretical considerations that different REVs for different properties should be expected (Baveye and Sposito, 1984; Bear and Braester, 1972). For example, Baveye et al. (2002) reported smaller REVs for air-filled pores than for the bulk density in two different subsoil volumes. Costanza-Robinson et al. (2011) found REVs for porosity, water saturation and air–water interfacial area, with each of the three investigated properties exhibiting a different average REV volume.

Almost all recent REV studies have evaluated the variation of X-ray imaged porosity with increasing measurement volumes. Such studies have been carried out for glass bead mixtures (Al-Raoush and Willson, 2005; Clausnitzer and Hopmans, 1999), rocks (Biswal et al., 1998; Brown et al., 2000) and soil (Baveye et al., 2002; Vogel et al., 2002). Authors of studies comparing different materials generally reported individual REVs for each specific material or sample (Al-Raoush and Papadopoulos, 2010; Baveye et al., 2002; Borges et al., 2018; Zhang et al., 2000). Pore networks in soils are strikingly different from those in rocks. The few studies investigating soil samples that we are aware of all found REVs for the imaged porosity. These ranged from scales larger than approximately 18 mm (Vogel et al., 2002; when the largest pores were excluded) to larger than approximately 26 mm (Borges et al., 2018) and 30 mm (Baveye and Sposito, 1984) for air filled pores, including some sub-resolution pores. Notably, the total number of investigated soil samples in these three studies are only 15 in total, with 12 of them investigated by Borges et al. (2018).

In comparison to studies focused on the porosity, studies investigating REVs for measures of connectivity are scarcer. We are aware of a few studies investigating REVs of the percolation probability P_p (Biswal et al., 1998; Keller et al., 2013), the connected porosity φ_c (Mu et al., 2016) and the percolation threshold p_c (Bruns et al., 2017; Keller et al., 2013), all of which were carried out on rocks. Studies on the connectivity of the soil pore space have evaluated the Euler density χ_n (mm^{-3}), i.e. the Euler-Poincaré characteristic normalized by the volume of the investigated ROI. Vogel et al. (2002) observed an REV for a volume larger 4500 mm^3, corresponding to a cubic edge length of approximately 16 mm. The single sample included in Vogel et al. (2002) was taken from the B-horizon of a loamy clay Cambisol. Borges et al. (2018), in contrast, found that the REV for χ_n was larger than the investigated soil volume of 50,193 mm^3 (cubic edge length of approximately 37 mm) for all 12 investigated soil columns. The samples were taken from the topsoil of a Rhodic Ferralsol, six samples from a no-

tillage plot and six from a conventionally tilled plot.

In this study, we aimed at further investigating the existence of REVs for porosity and connectivity metrics of soil pore networks. We focused on a scale that is typically used to measure soil hydraulic properties in laboratories, namely the small column scale with a volume of approximately 100 cm³. Beside the Euler density, we also included connectivity metrics from percolation theory. Connectivity metrics depend on the minimum considered pore diameter (Vogel et al., 2010). The connectivity of especially the large pores is critically important for both soil permeability (Koestel et al., 2018) and the occurrence of hydraulic non-equilibrium or preferential flow (Jarvis et al., 2016, 2017). We therefore performed the REV analyses for three different minimum pore diameters (80, 250 and 500 µm) in such a way that only the connectivity of pores larger than this minimum diameter was investigated. Finally, as any REV study entails detailed analyses of scale-dependence, our study also explores the scale-relationships of porosity and connectivity as a corollary.

2. Material and methods

2.1. Soil samples

25 aluminum cylinders (65 mm diameter, 60 mm height) were sampled at five different depths (see Table 1) from a soil profile in an agricultural field site in the Skuterud catchment, approximately 2.5 km east of Ås, Norway. They are a subset of the samples investigated in Koestel et al. (2018). At the time of sampling in November 2015, the field had been cropped with oats. The soil properties are summarized in Table 1.

2.2. X-ray imaging

We scanned the samples at the Department of Soil and Environment at the Swedish University of Agricultural Sciences in Uppsala (Sweden), using a GE v|tome|x 240 X-ray scanner with a tungsten target and a 16″ flat panel detector with a four megapixel resolution. We imaged the columns at tube voltages between 150 and 170 kV and electron flows between 300 and 600 µA. We did not use optical filters because the thick aluminum wall of the soil samples provided sufficient filtering of the low frequency X-rays. 2000 radiographs were taken for each 3-dimensional image with a voxel size of 0.04 mm in all directions. This approximately corresponds to a feature recognition of 0.08 mm size.

2.3. Image processing

We processed the 25 3-dimensional X-ray images using SoilJ (Koestel, 2018), a plugin for the open source software ImageJ/FIJI (Schindelin et al., 2012). The image processing steps that led to binary images of the pore network were identical to the ones described in Koestel et al. (2018). In short, we used SoilJ to detect the soil column outlines automatically. We then re-scaled the gray values in each individual 2-dimensional horizontal image cross-section between the 0.1 percentile and the gray value of the aluminum wall. Here, we exploited

Table 1
Mean soil properties at the sampling site.

Depth (cm)	Number of samples	Organic carbon content (%)	Bulk density (g/cm³)	Texture		
				Sand	Silt	Clay
7.5	6	2.17	1.33	0.240	0.479	0.281
22.5	4	2.05	1.35	0.246	0.492	0.262
32.5	7	1.21	1.43	0.256	0.501	0.244
52.5	4	0.38	1.67	0.227	0.524	0.249
72.5	4	0.18	1.67	0.265	0.543	0.192

the fact that air-filled pores occupied at least 0.1% of the imaged cross-section, therefore providing a calibration point for the gray-value corresponding to air. After all 3-D images had been calibrated to an identical gray-scale, we calculated the joint-histogram for all 25 images. Then we used the gray-value corresponding to the histogram minimum between the peaks corresponding to air and soil matrix as a threshold to binarize the images into air-filled pores and all denser imaged phases. In a final post-processing step, we removed all isolated pore clusters with an average pore diameter smaller than 0.08 mm. These isolated, thin clusters predominantly represent noise. Removing them has a similar effect as applying a median filter to the binarized images.

2.4. Analyses of pore network morphologies

The imaged pores approximately correspond to all pores with diameters larger than 80 µm, which roughly coincides with the size range for which macropores are commonly defined (SSSA, 2008). We therefore refer to them as macropores in the following. The macroporosity φ was calculated as the ratio of pore to total voxels in an ROI. We evaluated three connectivity metrics, the Euler-Poincaré density χ_n, the connection probability Γ (–) and the critical pore diameter d_c (mm). We obtained all three connectivity measures with SoilJ, using an implementation of MorphoLibJ (Legland et al., 2016) to calculate the Euler-Poincaré number χ.

The Euler-Poincaré characteristic χ and the connection probability Γ are both measures that quantify how well the pores in the investigated ROI are connected. However, neither χ nor Γ contains explicit information on whether there is a pore connection from the top to the bottom of the ROI. In our study, the Euler-Poincaré characteristic is the difference between the number of isolated pore clusters and the sum of loops (or redundant connections) in all these pore clusters. Theoretically, the number of cavities inside the pores also contribute to χ but since they would correspond to levitating soil particles, they remain zero in our case. The Euler-Poincaré characteristic χ is an extensive metric that scales with the volume of the considered ROI. To compare χ at the different investigated scales, we normalized it by the ROI-volume and refer to as the Euler density χ_n (mm⁻³). Negative χ_n values indicate well-connected pore networks, while positive values imply a larger number of isolated pore clusters.

The connection probability is defined as the probability for two pore voxels to be connected (i.e. belong to the same cluster, Renard and Allard, 2013; Jarvis et al., 2017):

$$\Gamma = \frac{\sum_{i=1}^{N} n_i^2}{\left(\sum_{i=1}^{N} n_i\right)^2} \tag{1}$$

where N (–) is the number of isolated pore clusters and n_i (-) the number of pore voxels contained in cluster i. A Γ value of one means that all pore voxels in the investigated ROI are connected to each other. The larger the number of isolated pore clusters and the smaller their size, the smaller Γ becomes. We assigned a value of zero to the connection probability if an ROI did not contain any pore cluster.

The connection probability Γ and the Euler density χ_n differ in that the former gives more weight to large connected clusters. It becomes large if most of the pore space comprises one single pore cluster. Such pore systems are likely to exhibit a percolating pathway from top to bottom (Stauffer and Aharony, 2014). Large values of Γ therefore indicate percolation (Jarvis et al., 2017). In contrast, the Euler density χ_n does not depend on the size of individual pore clusters and its value may be strongly influenced by small local features of the pore network, e.g. small pore clusters around plant residues that form a large number of redundant connections. χ_n is moreover more sensitive to image noise than Γ (Herring et al., 2015). Γ is therefore to be preferred as a quantitative measure (Renard and Allard, 2013). In this study we included χ_n to compare its scaling behavior with the ones found in previous work reported by Vogel et al. (2002) and Borges et al. (2018).

The critical pore diameter d_c is defined as the diameter of the largest sphere that can pass through the pore network, from the top to the bottom of the ROI. It is therefore a measure of the bottleneck pore diameter in the percolating pore space. It is a prime candidate for a characteristic length determining the permeability of porous media (Arns et al., 2005; Ghanbarian et al., 2016; Katz and Thompson, 1986; Koestel et al., 2018). We set d_c to the image voxel size of 0.04 mm for ROIs with non-percolating pore space.

2.5. Scale analyses

To define our domain of interest we first cut a $40 \times 40 \times 40$ mm^3 large cubic soil volume from the center of each of the 25 binary 3-D images. The criterion of limited changes in the effective property when increasing volume should hold for any random position in the domain of interest. Due to limitations in the size of our domains of interest, it is not practical to sample randomly. Instead, we used a volume sampling method to analyze REVs, similar to the second method described in Brown et al. (2000). In short, we expanded a cubic ROI anchored at one of the eight corners of the entire $40 \times 40 \times 40$ mm^3 investigated volume. We evaluated ROIs of 13 different sizes covering the range of scales between 5 and 40 mm, namely with edge lengths L of 5, 5.7, 6.6, 8, 10, 13.3, 17.8, 20, 22.2, 26.7, 31.1, 35.6 and 40 mm (Fig. 1). In each of the 13 ROIs we measured the macroporosity φ and the three connectivity measures χ_n, Γ, and d_c. Next, we repeated this procedure for each of the seven remaining corners of the entire investigated cube. As a result, we obtained eight scale relationships for each soil sample and morphological measure. It is clear that only the eight smallest ROI sizes yield mutually independent results. For the five largest ROI sizes, overlaps occur (see Fig. 1) that cause the macroporosity and connectivity measures in the investigated ROIs to converge.

We repeated the above-described procedure using images of pore systems from which all features with a diameter of less than 0.25 mm had been removed. We created these images by first quantifying the imaged pore diameters in each image by applying the maximal inscribed sphere method. Thereafter, we carried out the same scale-
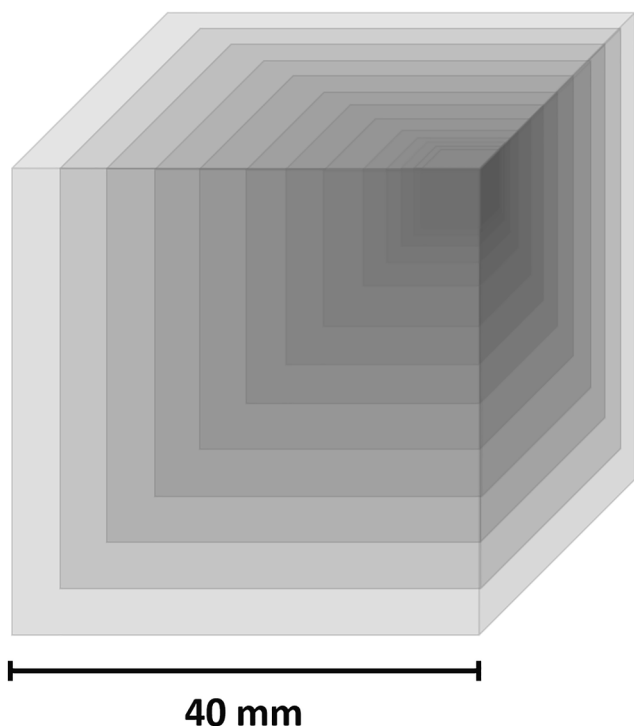
analyses a third time, on pore network images from which we had erased all features with diameters smaller than 0.5 mm. An illustration of the effect of the minimum considered pore diameter on the pore network is given in Fig. 2.

2.6. REV analyses

2.6.1. Lower REV boundary

In our study, we followed an approach to investigate the lower boundary l_{min} of potentially existing REVs that was suggested by Bear and Braester (1972) and slightly modified by Li et al. (2009). For the estimation of REVs around our 8 points in each domain of interest, we calculated the relative gradient with increasing ROI of the variable Y, which symbolizes one of the four investigated morphological properties, i.e. φ, χ_n, Γ and d_c:

$$\nabla Y = \frac{2 |Y_{i+1} - Y_i|}{(Y_{i+1} + Y_i)(L_{i+1} - L)} \tag{2}$$

where the index i stands for one of the first 12 investigated ROI sizes and index i + 1 for the next larger one. Note that we used $\log_{10} d_c$ in (2) to account for the heavily right-skewed distribution of d_c. As previous studies have done, we defined an ad-hoc threshold of $\nabla Y \leq 0.1$ for which the assumption of a point REV at the respective scale holds. We included an additional criterion, namely that all eight investigated ROIs must remain below the ad-hoc threshold of $\nabla Y \leq 0.1$. Scales at which only one of the eight investigated REVs exhibited $\nabla Y > 0.1$ were not labelled as an REV. In this fashion, we made sure that we selected the smallest scale for which the REV requirement was fulfilled in the entire investigated volume. As discussed above, the ROIs in our study with L > 20 mm exhibit an artificial reduction of variation of ∇Y as the eight ROIs are then overlapping. Detected REVs for ROIs with L > 20 therefore need to be interpreted with care. Fig. 3 illustrates how we investigated the existence of REVs using only the criterion of $\nabla Y \leq 0.1$.

2.6.2. Upper REV boundary

In cases for which a lower REV boundary $l_{min} \leq 20$ mm was found, we estimated upper REV boundaries l_{max} as proposed by Bachmat and Bear (1986). Their approach builds upon the assumption that for small distances, drifts in morphological properties Y are well approximated by a linear relationship. Then, the absolute value of the gradient in the bulk soil property $|gradY|$ is used to estimate l_{max} as follows:

$$l_{max} = \frac{2E(Y)}{|gradY|} \delta \tag{3}$$

where E(Y) is the expected value of any statistical moment of the soil property Y, i.e. its mean value, and

$$\delta = \frac{|\Delta \widehat{Y}|_{l_{max}}}{E(Y)} \tag{4}$$

with $|\Delta \widehat{Y}|_{l_{max}}$ being the difference in any statistical moment of the property between adjacent regions with sizes of l_{max}. In other words, δ is the largest relative deviation that is tolerable for the existence of an REV. For the sake of simplicity, we will only consider the first statistical moment, i.e. the mean value of Y, when estimating l_{max}. To give an example, the upper REV boundary for the macroporosity would be estimated from the macroporosities in the eight ROIs with edge lengths L just larger than l_{min}. First of all, we used a threshold value of 0.2 for δ. The eight ROIs served to calculate E(φ) and yield 28 permutations for pairs for which *grad* φ can be calculated and hence 28 estimations of l_{max}. These we combined to an average estimate for the upper REV boundary by taking their mean value as E(l_{max}).

2.6.3. Statistical homogeneity

As we are not aware of any study using the l_{max} estimation method outlined above, we additionally calculated the CV as a simple measure

Fig. 1. Schematic figure of the thirteen investigated ROI sizes anchored at the upper right front corner of the largest ROI ($40 \times 40 \times 40$ mm^3).
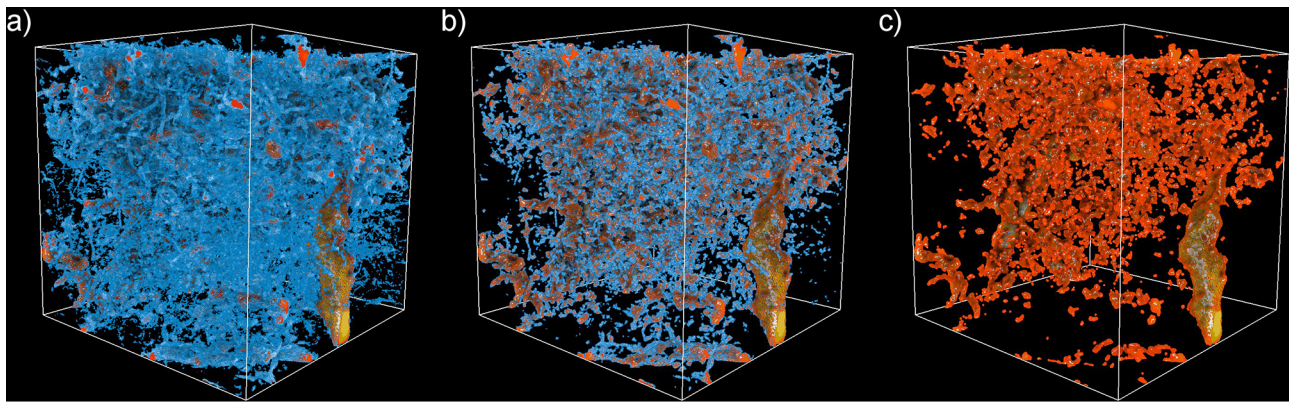
40 mm

Fig. 2. Illustration of the effect of the minimum considered pore diameter on the pore network of a column sampled at 22.5 cm depth, which is a) 80 μm, b) 250 μm and c) 500 μm. The $40 \times 40 \times 40$ mm³ ROI is shown. Blue colors indicate pores with diameters smaller than 500 μm, red and yellow colors diameters equal or larger than 500 μm. Note that the color scheme were slightly adjusted for each of the three images to high-light differences in the considered pore space. (For interpretation of the references to color in this figure legend, the reader is referred to the web version of this article.)

for evaluating the statistical homogeneity inside potential REVs, as it has been frequently done in the literature (e.g. Brown et al., 2000; Bruns et al., 2017; Zhang et al. 2000). In this way, we provide a measure that allows for better comparability with the results of previous studies. Following Zhang et al. (2000), we investigated whether the coefficient of variation CV(Y) of the eight ROIs in a sample was smaller than a threshold value of 0.2. The edge lengths L of the investigated samples were required to be larger than or equal to l_{min} but smaller than or equal to 20 mm, which is the largest edge length that yields non-overlapping ROIs.

Note that we did not attempt to identify more than one REV scale range as proposed by Vogel and Roth (2003), since our data does not cover a sufficient range of scales to allow for such an analysis.

3. Results and discussion

3.1. Pore network morphology

Fig. 4 illustrates the investigated morphological properties summarized by sampling depth. The samples taken at 22.5 cm depth exhibit the largest macroporosities and the largest connection probabilities Γ and smallest χ_n. We had expected that the largest and best-connected macropore structures would be located in the topsoil, where biological (e.g. earthworm burrowing, root growth) and physical processes (e.g. wetting/drying, freezing/thawing) that generate and maintain macrostructure are most pronounced. Samples taken at 7.5 cm depth most likely showed less well-developed macropore structures because they were sampled underneath wheel tracks where the surface soil was compacted. This is also likely the reason why the samples from the uppermost layer exhibit the largest variance in most of the observed morphological properties. The largest critical pore diameters d_c were found at depths of 32.5 and 52.5 cm. We suspect that this is due to the presence of biopores that were not destroyed by repeated traffic and tillage operations, as they are located below plough depth. As expected, the samples from 72.5 cm depth show the lowest porosity φ, connection probability Γ and critical pore diameter d_c. At this depth, the porosity is reduced by overburden pressure, while biological activity is less pronounced and physical processes that create macrostructure are largely absent.

Fig. 4 also displays how the morphological properties were affected by the choice of minimum pore diameter. The porosity φ decreases as the smaller pores were removed and thus so does the connection probability Γ. The latter indicates that the smallest pores $(0.08 \leq d < 0.25$ mm$)$ help to connect the larger macropores to larger pore clusters. Interestingly, Γ increased again after we removed also the

next largest pore diameter class $(0.25 \leq d < 0.5$ mm$)$. Apparently, these medium-sized macropores do not contribute much to connecting the largest macropores, but instead tended to form smaller, isolated pore clusters. The trend towards a less connected pore network for larger minimum pore diameters was only occasionally reflected in the Euler densities χ_n, namely for the sampling depth of 22.5 cm. Otherwise, the Euler density was always largest when all imaged pore sizes were considered. With all pores smaller than 0.25 mm diameter removed, the Euler density became negative for all samples. Obviously, many small, isolated pore clusters that did not contain any loops existed in most of the soil samples. When these clusters were removed, the number of loops outweighed the number of clusters, despite the decreased pore connectivity indicated by a drop in Γ. An increase in χ_n when only considering the largest pores $(d \geq 0.5$ mm$)$ indicated that the largest macropores did not form many redundant connections. This suggests that the largest pores were biopores as faunal burrows or root channels are unlikely to exhibit many loops (Capowiez et al., 2011; Pagenkemper et al., 2015).

3.2. Scale relationship of pore network morphology

The mean macroporosity φ of all 25 soil samples remained approximately constant with scale, irrespective of the considered minimum pore diameter (Fig. 5). The scale-relationships of the mean values of the connectivity measures Γ, χ_n and d_c were more variable. The mean Γ increased slightly towards the largest investigated ROI when all imaged pores were included, but decreased drastically with scale when we removed the pores with diameters smaller than 0.25 mm. Again, we attribute this to the important role of the smallest imaged pore class in connecting clusters with larger pores into one large cluster. At small scales, a single cluster may still dominate most of the pore space, resulting in a relatively large Γ. However, as the scale increased, an ROI captured several unconnected medium-sized clusters, which leads to small Γ.

The mean Euler density χ_n decreased from slightly positive values at the smallest investigated scale to relatively constant negative values at scales of L > 20 mm when all imaged pores were included. We suspect that this trend was observed because a few strongly negative values of the Euler density from soil samples from 22.5 cm depth influenced the mean values disproportionately (see Fig. 4c). The trend in mean Euler densities with scale is nevertheless consistent with the trend in Γ, indicating larger connected pore clusters with increasing scale, connected by pores with diameters < 0.25 mm. The latter follows from the approximately constant Euler densities χ_n with scale after removing the smallest pores. Finally, the mean critical pore diameter d_c steadily

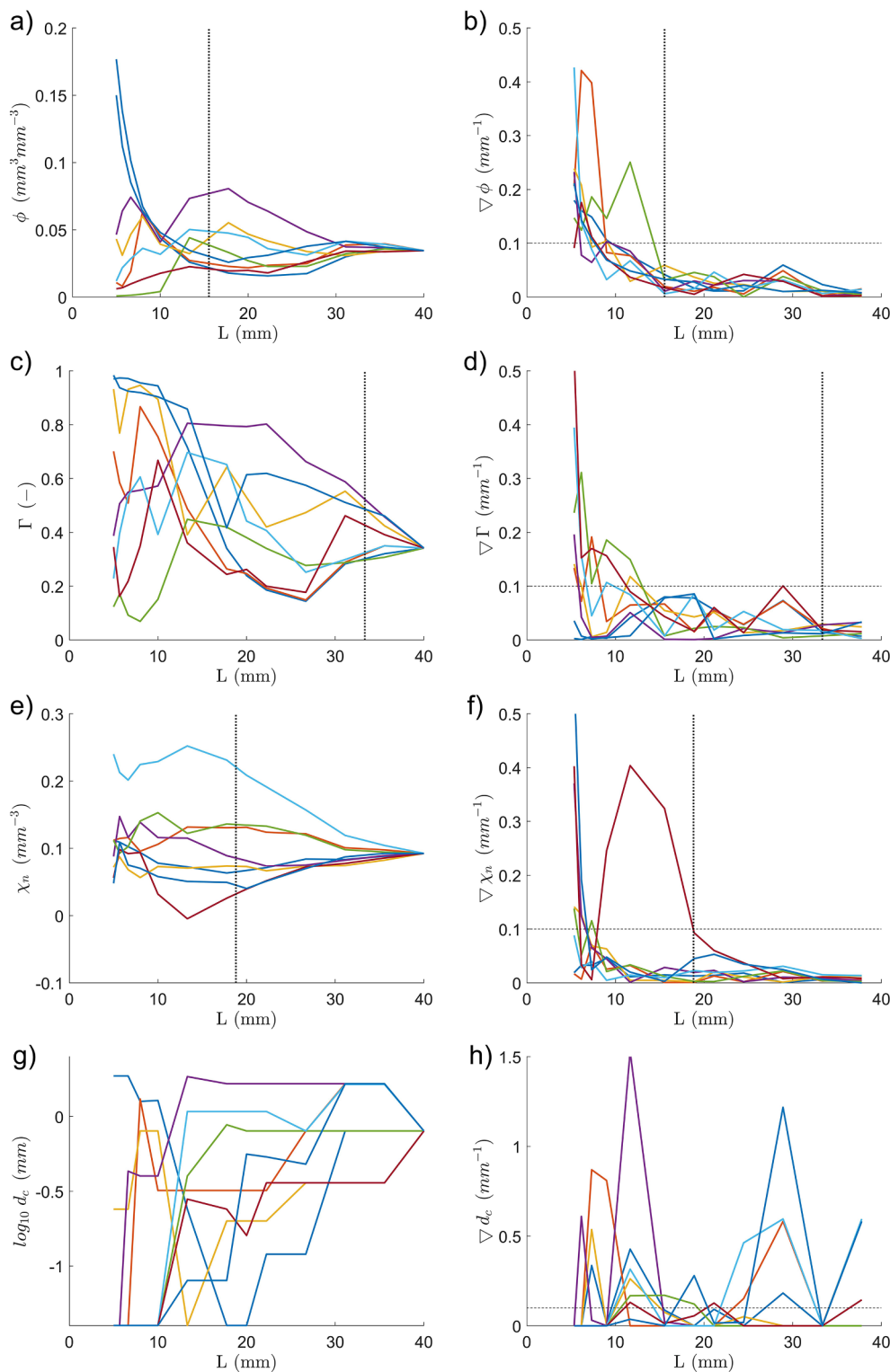**Fig. 3.** Scale-relationships for column 12 (sampling depth 32.5 cm) as an example illustrating how an REV for the $40 \times 40 \times 40$ mm^3 domain of interest was detected. All pores larger than 0.08 mm were considered in this figure. Each color denotes one of the eight ROI-series per soil sample. On the left, the development of the morphological properties with scale is depicted as they converge to the value of the largest investigated ROI. The right hand panel shows the respective relative gradients. The horizontal dashed-line indicates the relative gradient threshold of 0.1 below which an ROI is considered an REV. The lower REV bound is depicted as the vertical dotted line. No lower REV bound was found for the critical pore diameter d_c for this column.

increased with scale, reflecting an increasing probability of capturing an ever-larger pore in the percolating pore space for larger and larger ROIs.

The standard deviation of the macroporosity φ decreased rapidly with scale for L < 15 mm (Fig. 5a) and moderately between scales of 15 mm ≤ L < 30 mm. Beyond L = 30 mm it was approximately constant with scale, reflecting the effect of the increasing overlap of the eight investigated ROIs for L > 20 mm (Fig. 5a). This was different for the three investigated connectivity measures (Fig. 5). The standard deviation for Γ and χ_n remained approximately constant with scale unless only pores with d ≥ 0.5 mm were considered, for which they both decreased slightly and approximately linearly with increasing scale over the entire investigated scale range. In contrast, the standard deviation of d_c increased with scale. It follows that the in-between
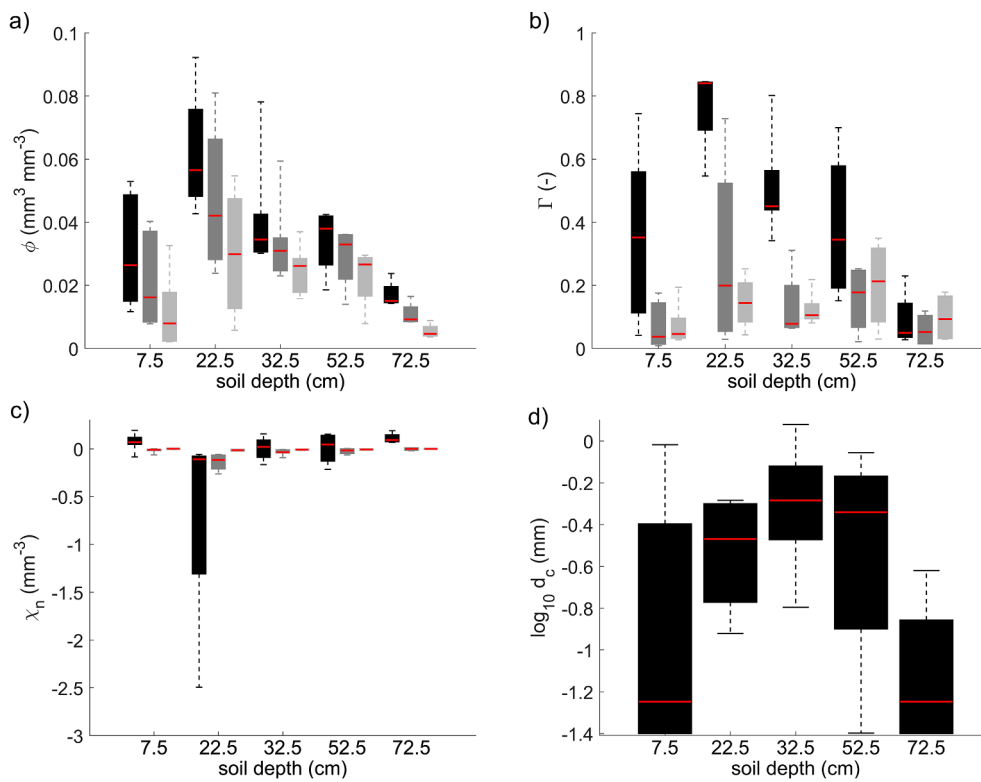
a)

b)

c)

d)

Fig. 4. Overview over the morphologic properties of the largest investigated ROI of all 25 soil samples for the 5 different sampling depths. The upper and lower edges of the boxplot bodies correspond the upper and lower quartile of the observed values, the extreme values to the respective maximum and minimum values. The red line marks the median value. The gray-scale denotes the minimum considered pore diameter: 0.08 mm (black), 0.25 mm (dark gray), 0.5 mm (light gray). (For interpretation of the references to color in this figure legend, the reader is referred to the web version of this article.)
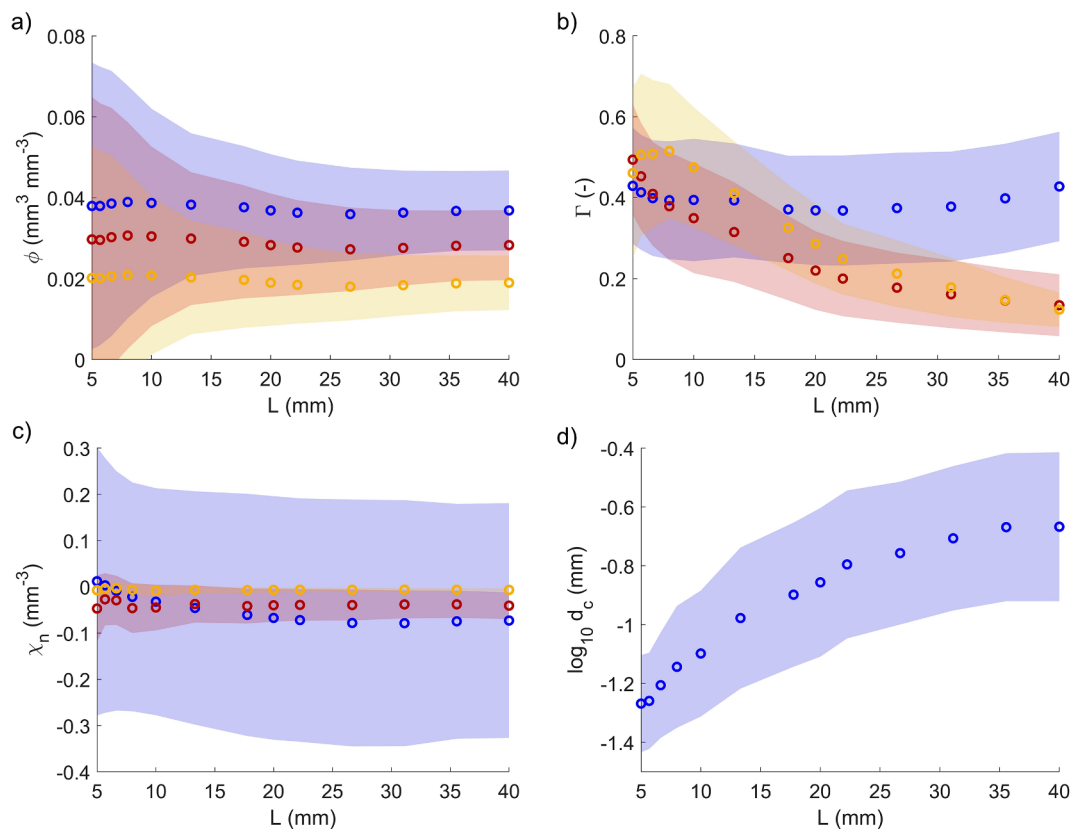
a)

b)

c)

d)

Fig. 5. Scale dependence of the four investigated morphologic properties. Circles refer to the mean value of all 25 columns. The width of the accompanying cloud corresponds to the respective standard deviation. The color-scale denotes the minimum considered pore diameter, i.e. 0.08 mm (blue), 0.25 mm (red), 0.5 mm (yellow). (For interpretation of the references to color in this figure legend, the reader is referred to the web version of this article.)
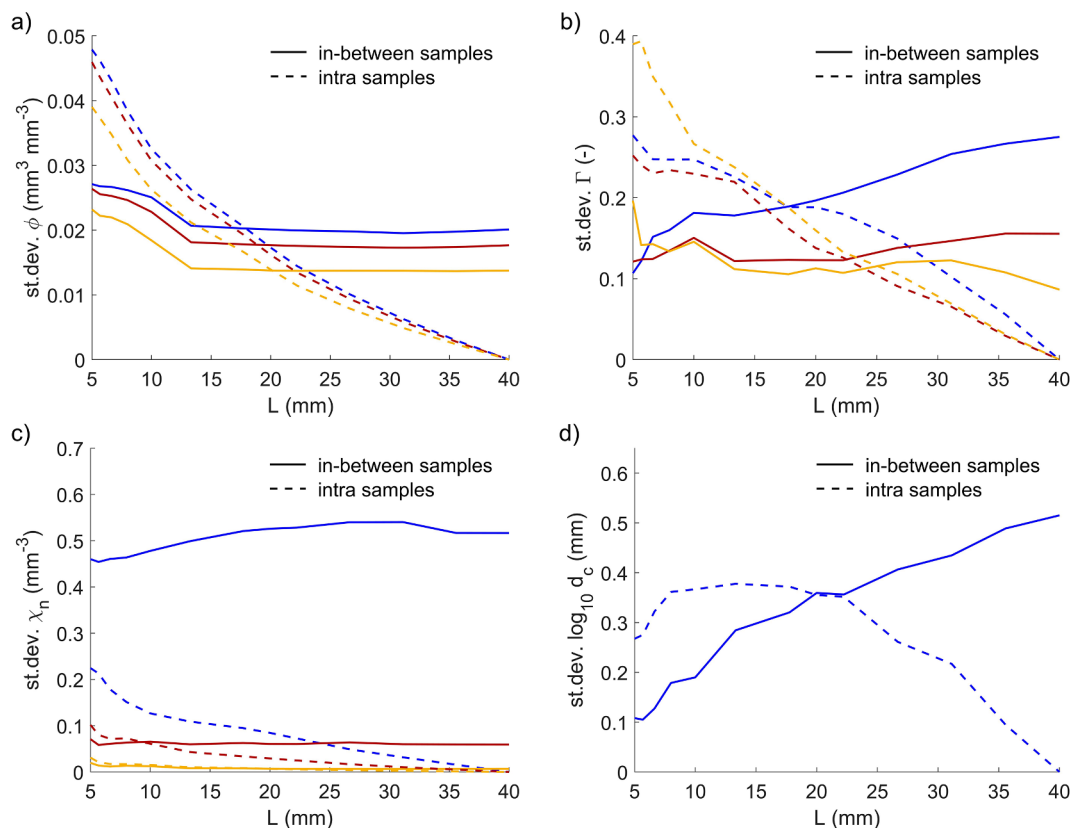
Fig. 6. Scale dependence of the standard deviation of the intra sample means (between samples) and the mean of the intra-sample standard deviations (intra sample) of the four investigated morphologic properties. The color-scale denotes the minimum considered pore diameter, i.e. 0.08 mm (blue), 0.25 mm (red), 0.5 mm (yellow). (For interpretation of the references to color in this figure legend, the reader is referred to the web version of this article.)

sample variance for the connectivity measures was increasing with scale while the intra-sample variance was decreasing due to the ROI-overlap as demonstrated by Fig. 6b,c and d. The relative magnitude of the standard deviation decreased with the minimum considered pore diameters, linearly for φ and Γ and exponentially for χ_n. The latter was maybe caused by the large sensitivity of χ_n to local small-scale connectivity features.

3.3. REV analyses

3.3.1. Lower REV boundary

It is clear from Fig. 3 that the investigated effective properties occasionally showed large differences even at the scale of 20 mm, which is the edge length of the largest non-overlapping ROI. This is consistent with observations made by Baveye et al. (2002). For sample #12 (Fig. 3), the macroporosity φ varied by more than a factor of three, the connection probability Γ spanned values between 0.25 and 0.8 and the critical pore diameter d_c ranged from less than 0.08 to more than 1.5 mm, which is almost as large as the maximum observed range of d_c in all samples. However, these large variations in ROI pore network characteristics did not prevent the detection of lower bounds for REVs for most domains of interest and effective properties if only the criterion of $\nabla Y \leq 0.1$ for all 8 ROIs was applied. Accordingly, for sample #12, φ met the lower-bound REV criterion defined in this study at a scale of L = 15.5 mm, and the Euler density at L = 18.9 mm. A lower REV bound for Γ was only found at L = 33.3 mm, far into the domain where the investigated ROIs were overlapping.

The only pore-network property for which we predominantly found lower REV bounds at scales smaller than 20 mm was the macroporosity φ for d $\geq$ 0.08 mm with a median value of L = 15.5 mm (Fig. 7a).

Notably, this coincides with the slower decay of the standard deviation for L > 15 (Fig. 5a). This is in the range of values found by Vogel et al. (2002), but clearly smaller than the ones reported by Baveye et al. (2002) and Borges et al. (2018). However, different methods were used to detect REVs, which makes it difficult to compare results. A thorough analysis focusing on how the different REV detection methods perform and compare is still lacking in the peer-reviewed literature.

The lower REV boundary for φ increased with an increase in minimum considered pore diameters, i.e. d $\geq$ 0.08, d $\geq$ 0.25 and d $\geq$ 0.5. This reflects the hierarchical nature of soil pore networks in which larger pores are separated by larger distances than smaller pores. The scaling of the macroporosity lower REV bound with increasing minimum considered pore diameter was also visible at most individual sampling depths (Fig. 8a). Interestingly, the lower REV boundary for the macroporosity remained relatively constant with sampling depth in the soil profile.

All median lower-bound REV values for the investigated connectivity measures were larger than L = 20 mm, i.e. in the range in which the overlapping ROIs biased the results towards small ∇Y. This indicates that the edge lengths of REV lower bounds for Γ, χ_n and d_c could not be determined for most of the samples. In many cases, lower REV bounds were probably larger than 30 mm; some of them possibly even larger than 40 mm, if they even exist.

3.3.2. Upper REV boundary and statistical homogeneity

Fig. 9 shows that the mean estimated upper REV boundary E(l_{max}) for the macroporosity φ was always larger than the detected lower REV boundary l_{min}. The smaller E(l_{max}) that is observed when the ROIs with edge lengths L = 17.8 mm were used (Fig. 9a) may be related to the fact that these ROIs were only approximately adjacent to each other. E
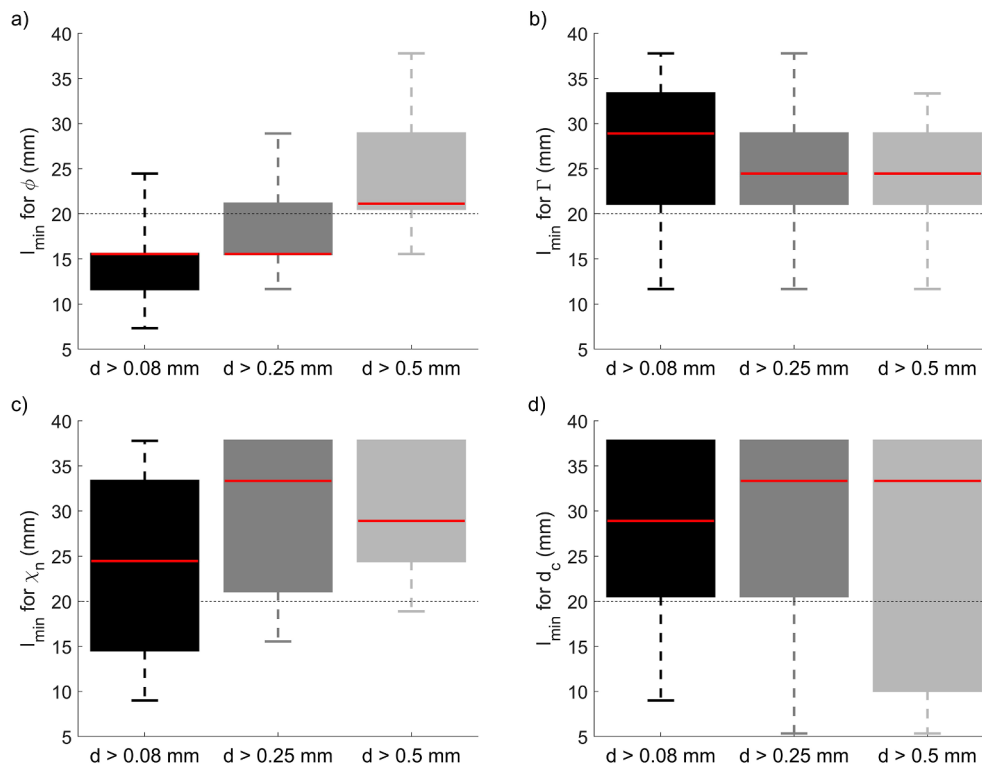
Fig. 7. Lower bounds for REVs detected for the four different morphologic properties in the 25 soil samples as a function of the minimum pore diameter. The criterion for the lower bound was $\nabla Y < 0.1$ for all 8 ROIs only. The upper and lower edges of the boxplot bodies correspond to the upper and lower quartiles of the observed values, and the extreme values to the observed maximum and minimum values. The edge length above which the eight ROIs overlap is indicated with a dashed line. The red line marks the median value. The gray-scale denotes the minimum considered pore diameter: 0.08 mm (black), 0.25 mm (dark gray), 0.5 mm (light gray). (For interpretation of the references to color in this figure legend, the reader is referred to the web version of this article.)

(l_{max}) calculated from the ROIs with an edge length of L = 20 mm (Fig. 9b) may therefore represent more robust estimations. According to Eq. (3), the investigated soil samples exhibit an REV range for the macroporosity φ between scales of L $\approx$ 15 mm and L $\approx$ 60 mm. Notably, a decrease of l_{max} with an increase in the minimum considered pore diameter was found (Fig. 9). E(l_{max}) decreased from a median value of 65.9 to 59.8 to 42.7 mm for minimum diameters of 0.08, 0.25 and 0.5 mm. Together with the increase of l_{min} (Fig. 7) with the minimum considered pore diameter, it appears that REV ranges for porosity are narrower when only larger pores are considered. At the same time, the trends in l_{min} and l_{max} with minimum pore size illustrate that the X-ray image resolution has a considerable impact on the results of scaling analyses.

The criterion for statistical homogeneity of a coefficient of variation between the eight ROIs of smaller than 0.2 is, however, not fulfilled for any sample with L $\geq$ l_{min} (Fig. 10). It is unclear which of the two measures for statistical homogeneity (i.e. the estimated upper REV boundary E(l_{max}), or the coefficient of variation) is better suited for detecting REVs.

4. Conclusions

While the mean imaged porosity remained approximately constant with scale irrespective of the minimum considered pore diameter, the investigated connectivity measures did not. Instead, we found improved connectivity with larger scale when all the imaged pore space was considered, whereas the connectivity of pores larger than 0.25 mm decreased with scale. Thus, pores with diameters between 0.08 and 0.25 mm were of fundamental importance in connecting larger, otherwise isolated macropores. This stresses the importance of the

image resolution when conducting scale analyses for connectivity measures. The critical pore diameter steadily increased with scale, probably due to an increased probability of encompassing a continuous, vertical biopore within the sample. In addition, the standard deviation of the critical pore diameter likewise increased with scale, reflecting an also larger probability that an otherwise well-connected macropore network is clogged at a critical position.

We found a median lower REV-bound for the macroporosity of 15.5 mm in the investigated soil samples when all imaged pores were considered. The lower REV-bounds detected for the investigated connectivity measures, i.e. the connection probability, the Euler density and the critical pore diameter were close to the total investigated soil volume of 40 × 40 × 40 mm³. This suggests that these values were most likely underestimated. Based on our results we conclude that larger soil samples should be used to measure soil properties and investigate processes that depend on the pore network connectivity, such as permeability or water flow and long-range solute transport. This is consistent with reports of scale dependence of hydraulic conductivity (Cunliffe et al., 2013; Jorda et al., 2015; Pachepsky et al., 2014), apparent dispersivity (Koestel et al., 2012; Vanderborght and Vereecken, 2007) and the strength of preferential flow (Koestel and Jorda, 2014).

We estimated a median upper REV boundary for the macroporosity of 65.9 mm when all imaged pores were considered. For the macroporosity, we therefore found an REV range between approximately 15 and 65 mm. The detected REV range was sensitive to the image resolution. If only pores with diameters of more than 0.25 mm were considered, the REV range decreased to a scale range between 18 and 60 mm. For pore diameters larger 0.5 mm, the range decreased further. However, the coefficients of variation of the macroporosity for ROIs within the REV range were clearly larger than a threshold value
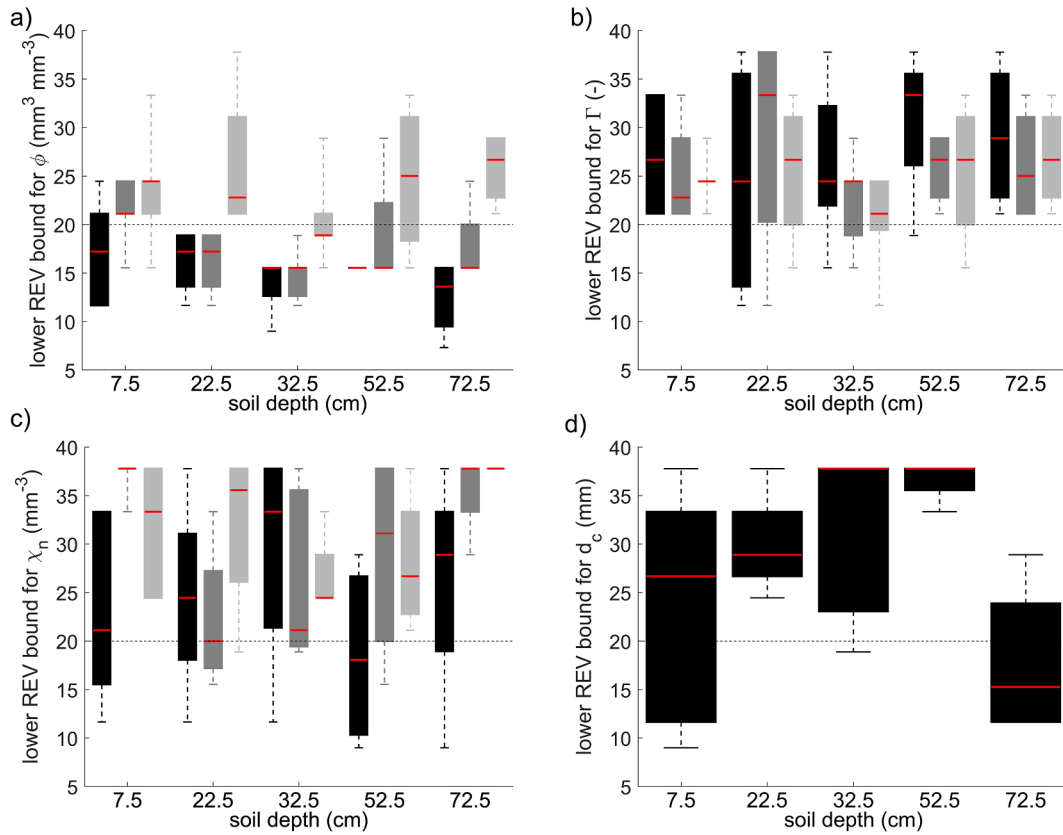
Fig. 8. Lower bounds for REVs for the effective macroporosity in dependence to the depth. The upper and lower edges of the boxplot bodies correspond the upper and lower quartile of the observed values, the extreme values to the respective maximum and minimum values. The red line marks the median value. The edge length above which the eight ROIs overlap is indicated with a dashed line. The gray-scale denotes the minimum considered pore diameter: 0.08 mm (black), 0.25 mm (dark gray), 0.5 mm (light gray). (For interpretation of the references to color in this figure legend, the reader is referred to the web version of this article.)

commonly used in the literature. This indicates that the macroporosity cannot be considered as statistically homogeneous within the above-detected REV range, which casts doubts on its existence. Whether a small coefficient of variation between ROIs is a necessary criterion for an REV and whether the estimation approach for the upper REV boundary is meaningful should be further investigated in future studies. A possible outcome of such studies may be that REVs are not wide-spread in soils, which would suggest that flow and transport models that explicitly account for heterogeneity are necessary.

In future studies, the hydraulic and transport properties emerging from the pore structures could also be investigated using numerical simulations based on direct X-ray measurements. Examples of this approach have already been published (e.g. Ozelim and Cavalcante, 2018; Zambrano et al., 2017; Zhang et al., 2000). For now, these studies have included very few samples, because of the computational demands. Nevertheless, with the prospect of future developments in computing hardware, such an approach is highly promising to increase our knowledge of how soil pore structures and soil functions are linked with scale.
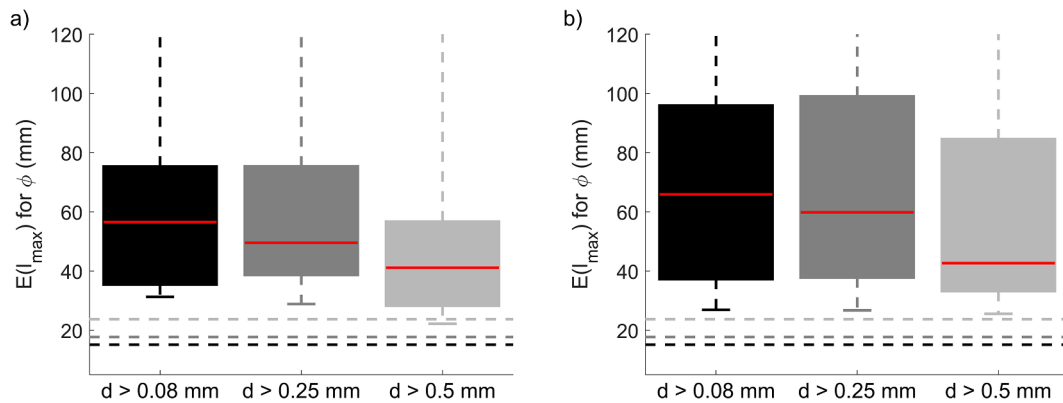

Fig. 9. Estimation for the mean upper REV boundary $E(l_{max})$ for the macroporosity φ based upon the ROIs with an edge length of a) 17.8 mm and with and edge length of b) 20 mm. The upper and lower edges of the boxplot bodies correspond the upper and lower quartile of the observed values, the extreme values to the respective maximum and minimum values. The red line marks the median value. The gray-scale denotes the minimum considered pore diameter: 0.08 mm (black), 0.25 mm (dark gray), 0.5 mm (light gray). The dashed lines mark the lower REV boundary l_{min} for each considered minimum pore diameter. (For interpretation of the references to color in this figure legend, the reader is referred to the web version of this article.)
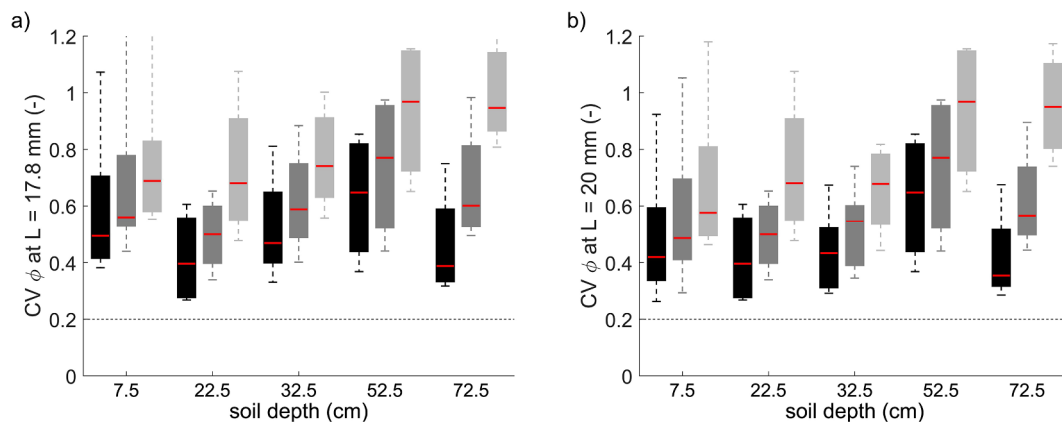
Fig. 10. The coefficients of variations for the effective macroporosity for the eight sub-ROIs at an edge length of a) 17.8 and b) 20 mm. The criterion of a CV < 0.2 for which the statistical homogeneity is sufficiently small is depicted as a dashed line. The gray-scale denotes the minimum pore diameter: 0.08 mm (black), 0.25 mm (dark gray), 0.5 mm (light gray).

Declaration of Competing Interest

The authors declare that they have no known competing financial interests or personal relationships that could have appeared to influence the work reported in this paper.

Appendix A. Supplementary data

Supplementary data to this article can be found online at https://doi.org/10.1016/j.geoderma.2020.114206.

References

Al-Raoush, R., Papadopoulos, A., 2010. Representative elementary volume analysis of porous media using X-ray computed tomography. Powder Technol. 200 (1–2), 69–77.

Al-Raoush, R.I., Willson, C.S., 2005. Extraction of physically realistic pore network properties from three-dimensional synchrotron X-ray microtomography images of unconsolidated porous media systems. J. Hydrol. 300 (1–4), 44–64.

Arns, C.H., Knackstedt, M.A., Martys, N.S., 2005. Cross-property correlations and permeability estimation in sandstone. Phys. Rev. E 72 (4).

Bachmat, Y., Bear, J., 1986. Macroscopic modelling of transport phenomena in porous media. 1: the continuum approach. Transp. Porous Media 1, 213–240.

Baveye, P., Rogasik, H., Wendroth, O., Onasch, I., Crawford, J.W., 2002. Effect of sampling volume on the measurement of soil physical properties: simulation with x-ray tomography data. Meas. Sci. Technol. 13 (5), 775–784.

Baveye, P., Sposito, G., 1984. The operational significance of the continuum-hypothesis in the theory of water-movement through soils and aquifers. Water Resour. Res. 20 (5), 521–530.

Bear, J., Braester, C., 1972. On the flow of two immiscible fluids in fractured porous media, in: Iahr (Ed.), Developments in soil science. Elsevier, pp. 177–202.

Berg, C.F., 2014. Permeability description by characteristic length, tortuosity, constriction and porosity. Transp. Porous Media 103 (3), 381–400.

Beven, K., Germann, P., 1982. Macropores and water flow in soils. Water Resour. Res. 18 (5), 1311–1325.

Biswal, B., Manwart, C., Hilfer, R., 1998. Three-dimensional local porosity analysis of porous media. Phys. A 255 (3–4), 221–241.

Borges, J.A.R., Pires, L.F., Cássaro, F.A.M., Roque, W.L., Heck, R.J., Rosa, J.A., Wolf, F.G., 2018. X-ray microtomography analysis of representative elementary volume (REV) of soil morphological and geometrical properties. Soil Tillage Res. 182, 112–122.

Brown, G.O., Hsieh, H.T., Lucero, D.A., 2000. Evaluation of laboratory dolomite core sample size using representative elementary volume concepts. Water Resour. Res. 36 (5), 1199–1207.

Bruns, S., Stipp, S.L.S., Sorensen, H.O., 2017. Statistical representative elementary volumes of porous media determined using greyscale analysis of 3D tomograms. Adv. Water Resour. 107, 32–42.

Buchter, B., Hinz, C., Flühler, H., 1994. Sample size for determination of coarse fragment content in a stony soil. Geoderma 63 (3), 265–275.

Capowiez, Y., Sammartino, S., Michel, E., 2011. Using X-ray tomography to quantify earthworm bioturbation non-destructively in repacked soil cores. Geoderma 162 (1–2), 124–131.

Clausnitzer, V., Hopmans, J.W., 1999. Determination of phase-volume fractions from tomographic measurements in two-phase systems. Adv. Water Resour. 22 (6), 577–584.

Costanza-Robinson, M.S., Estabrook, B.D., Fouhey, D.F., 2011. Representative elementary volume estimation for porosity, moisture saturation, and air-water interfacial areas in unsaturated porous media: data quality implications. Water Resour. Res. 47 (7).

Cunliffe, A.M., Baird, A.J., Holden, J., 2013. Hydrological hotspots in blanket peatlands: spatial variation in peat permeability around a natural soil pipe. Water Resour. Res. 49 (9), 5342–5354.

Ghanbarian, B., Torres-Verdín, C., Skaggs, T.H., 2016. Quantifying tight-gas sandstone permeability via critical path analysis. Adv. Water Resour. 92, 316–322.

Herring, A.L., Andersson, L., Schluter, S., Sheppard, A., Wildenschild, D., 2015. Efficiently engineering pore-scale processes: the role of force dominance and topology during nonwetting phase trapping in porous media. Adv. Water Resour. 79, 91–102.

Hubbert, M.K., 1956. Darcys law and the field equations of flow of the underground. Transact. Am. Inst. Mining Metallurgical Eng. 207 (10), 223–239.

Jarvis, N., Koestel, J., Larsbo, M., 2016. Understanding preferential flow in the vadose zone: Recent advances and future prospects. Vadose Zone J. 15.

Jarvis, N., Larsbo, M., Koestel, J., 2017. Connectivity and percolation of structural pore networks in a cultivated silt loam soil quantified by X-ray tomography. Geoderma 287, 71–79.

Jorda, H., Bechtold, M., Jarvis, N., Koestel, J., 2015. Using boosted regression trees to explore key factors controlling saturated and near-saturated hydraulic conductivity. Eur. J. Soil Sci. 66 (4), 744–756.

Katz, A.J., Thompson, A.H., 1986. Quantitative prediction of permeability in porous rock. Physical Rev. B 34 (11), 8179–8181.

Keller, L.M., Holzer, L., Schuetz, P., Gasser, P., 2013. Pore space relevant for gas permeability in Opalinus clay: statistical analysis of homogeneity, percolation, and representative volume element. J. Geophys. Res. Solid Earth 118 (6), 2799–2812.

Koestel, J., 2018. SoilJ: an ImageJ plugin for the semiautomatic processing of three-dimensional X-ray images of soils. Vadose Zone J. 17 (1).

Koestel, J., Dathe, A., Skaggs, T.H., Klakegg, O., Ahmad, M.A., Babko, M., Giménez, D., Farkas, C., Nemes, A., Jarvis, N., 2018. Estimating the permeability of naturally structured soil from percolation theory and pore space characteristics imaged by X-Ray. Water Resour. Res. 4 (11), 9255–9263.

Koestel, J., Jorda, H., 2014. What determines the strength of preferential transport in undisturbed soil under steady-state flow? Geoderma 217–218, 144–160.

Koestel, J., Larsbo, M., 2014. Imaging and quantification of preferential solute transport in soil macropores. Water Resour. Res. 50 (5), 4357–4378.

Koestel, J.K., Moeys, J., Jarvis, N.J., 2012. Meta-analysis of the effects of soil properties, site factors and experimental conditions on solute transport. Hydrol. Earth Syst. Sci. 16 (6), 1647–1665.

Köhne, J.M., Köhne, S., Simunek, J., 2009. A review of model applications for structured soils: a) Water flow and tracer transport. J. Contam. Hydrol. 104 (1–4), 4–35.

Lauren, J.G., Wagenet, R.J., Bouma, J., Wosten, J.H.M., 1988. Variability of saturated hydraulic conductivity in a glossaquic hapludalf with macropores. Soil Sci. 145 (1), 20–28.

Legland, D., Arganda-Carreras, I., Andrey, P., 2016. MorphoLibJ: integrated library and plugins for mathematical morphology with ImageJ. Bioinformatics 32 (22), 3532–3534.

Li, J.H., Zhang, L.M., Wang, Y., Fredlund, D.G., 2009. Permeability tensor and representative elementary volume of saturated cracked soil. Can. Geotech. J. 46 (8), 928–942.

Mu, Y., Sungkorn, R., Toelke, J., 2016. Identifying the representative flow unit for capillary dominated two-phase flow in porous media using morphology-based pore-scale modeling. Adv. Water Resour. 95, 16–28.

Ozelim, L., Cavalcante, A.L.B., 2018. Representative elementary volume determination for permeability and porosity using numerical three-dimensional experiments in microtomography data. Int. J. Geomech. 18 (2), 11.

Pachepsky, Y.A., Guber, A.K., Yakirevich, A.M., McKee, L., Cady, R.E., Nicholson, T.J., 2014. Scaling and pedotransfer in numerical simulations of flow and transport in soils. Vadose Zone J. 13 (12), -.

Pachepsky, Y., Hill, R.L., 2017. Scale and scaling in soils. Geoderma 287, 4–30.

Pagenkemper, S.K., Athmann, M., Uteau, D., Kautz, T., Peth, S., Horn, R., 2015. The effect of earthworm activity on soil bioporosity – investigated with X-ray computed tomography and endoscopy. Soil Tillage Res. 146, 79–88.

Raats, P.A.C., Klute, A., 1968a. Transport in soils – balance of mass. Soil Sci. Soc. Am. Proc. 32 (2), 161–166.

Raats, P.A.C., Klute, A., 1968. Transport in soils – balance of momentum. Soil Sci. Soc. Am. Proc. 32 (4), 452–456.

Renard, P., Allard, D., 2013. Connectivity metrics for subsurface flow and transport. Adv. Water Resour. 51, 168–196.

Sammartino, S., Lissy, A.-S., Bogner, C., Van Den Bogaert, R., Capowiez, Y., Ruy, S., Cornu, S., 2015. Identifying the functional macropore network related to preferential flow in structured soils. Vadose Zone J. 14 (10).

Scheibe, T.D., Perkins, W.A., Richmond, M.C., McKinley, M.I., Romero-Gomez, P.D.J., Oostrom, M., Wietsma, T.W., Serkowski, J.A., Zachara, J.M., 2015. Pore-scale and multiscale numerical simulation of flow and transport in a laboratory-scale column. Water Resour. Res. 51 (2), 1023–1035.

Schindelin, J., Arganda-Carreras, I., Frise, E., Kaynig, V., Longair, M., Pietzsch, T., Preibisch, S., Rueden, C., Saalfeld, S., Schmid, B., Tinevez, J.-Y., White, D.J., Hartenstein, V., Eliceiri, K., Tomancak, P., Cardona, A., 2012. Fiji: an open-source platform for biological-image analysis. Nat. Methods 9 (7), 676–682.

SSSA, 2008. Glossary of soil science terms 2008. Madison, WI: Soil Science Society of America.

Stauffer, D., Aharony, A., 2014. Introduction to percolation theory: revised second edition. CRC Press.

VandenBygaart, A.J., Protz, R., 1999. The representative elementary area (REA) in studies of quantitative soil micromorphology. Geoderma 89 (3–4), 333–346.

Vanderborght, J., Vereecken, H., 2007. Review of dispersivities for transport modeling in soils. Vadose Zone J. 6 (1), 29–52.

Vogel, H.-J., 2019. Scale issues in soil hydrology. Vadose Zone J. 18, 190001.

Vogel, H.J., Cousin, I., Roth, K., 2002. Quantification of pore structure and gas diffusion as a function of scale. Eur. J. Soil Sci. 53 (3), 465–473.

Vogel, H.J., Roth, K., 2003. Moving through scales of flow and transport in soil. J. Hydrol. 272 (1–4), 95–106.

Vogel, H.J., Weller, U., Schluter, S., 2010. Quantification of soil structure based on Minkowski functions. Comput. Geosci. 36, 1236–1245.

Wu, M., Wu, J., Wu, J., Hu, B.X., 2018. A three-dimensional model for quantification of the representative elementary volume of tortuosity in granular porous media. J. Hydrol. 557, 128–136.

Zambrano, M., Tondi, E., Mancini, L., Arzilli, F., Lanzafame, G., Materazzi, M., Torrieri, S., 2017. 3D Pore-network quantitative analysis in deformed carbonate grainstones. Mar. Pet. Geol. 82, 251–264.

Zhang, D.X., Zhang, R.Y., Chen, S.Y., Soll, V.E., 2000. Pore scale study of flow in porous media: scale dependency, REV, and statistical REV. Geophys. Res. Lett. 27 (8), 1195–1198.